

Slip length for a viscous flow over a plane with complementary lattices of superhydrophobic spots

Alexei T. Skvortsov^{a,*}, Denis S. Grebenkov^b, Leon Chan^c, Andrew Ooi^c

^a Defence Science and Technology Group, VIC 3207, Australia

^b Laboratoire de Physique de la Matière Condensée, CNRS – Ecole Polytechnique, Institut Polytechnique de Paris, 91120 Palaiseau, France

^c Department of Mechanical Engineering, The University of Melbourne, Parkville, VIC 3010, Australia

ARTICLE INFO

Keywords:

Microfluidics

Viscous fluid

Stokes flow

Effective boundary condition

ABSTRACT

We propose an approximation for the functional form of the slip length for two complementary lattice configurations of superhydrophobic texture. The first configuration consists of the square lattice of the superhydrophobic spots employed on the no-slip plane. The second configuration is an ‘inverse’ of the first one and consists of the same lattice but of the no-slip spots on the superhydrophobic base. We validate our analytical results by a numerical solution of Stokes equation.

1. Introduction

Shear flows over superhydrophobic (SHP) surfaces (surfaces containing regions of zero viscous stress) have gained increasing attention in recent years due to the remarkable ability of a hydrophobic coating to control flow and reduce hydrodynamic drag [1–3], which is important for the design of microfluidic devices (lab-on-chip) and numerous biomedical and maritime applications [4,5]. Mathematically, similar problems (viz., solution of the Laplace-type equations with mixed boundary conditions) emerge in the context of viscous flow over perforated membranes, diffusion kinetics, electrostatics, and models of wetting phenomena [6–10]. There is an extensive literature on analytical, numerical, and experimental results on this topic, see [4,6–9,11–23] and references therein. The comprehensive review which is relevant to the present study is given in Ref. [24].

One of the conventional ways to characterize the effect of SHP coatings is to introduce a lumped parameter λ in the effective boundary condition on the wet surface; this parameter is commonly referred to as the slip length [6]. In general, the slip length is a 2×2 tensor with only two non-zero diagonal values, λ_{\parallel} and λ_{\perp} [20]. When the SHP texture has the symmetry of a square lattice these values are equal: $\lambda_{\parallel} = \lambda_{\perp} = \lambda$. For a unidirectional flow over a flat boundary with the velocity vector along the side of the lattice cell (see Fig. 1) the effective boundary condition takes the form [4,6–9,11–25]

$$\lambda \frac{dv}{dz} = v, \quad (1)$$

where v is the component of velocity parallel to the boundary $z = 0$ (z is the distance to the boundary), the coordinate axes x, y are on the

boundary and are aligned with the square lattice, see Fig. 1. The limits $\lambda = 0$ and $\lambda = \infty$ correspond to a no-slip and a no-stress boundary, respectively.

There are many physical and chemical properties of the interface that determine the slip length such as liquid–gas interface deformation, internal gas flow, layer of surfactants, etc. (for further details see [24,25]). For the purpose of the present study we follow previous works [12,13] and assume that λ is completely defined by the surface fraction σ of the SHP spots (viz, the fraction of surface where tangential stress is zero), the shape of the individual spot, and their geometrical arrangements. As a function of σ , the parameter λ has two evident limits

$$\lambda \rightarrow 0, \quad \sigma \rightarrow 0, \quad (2)$$

$$\lambda \rightarrow \infty, \quad \sigma \rightarrow 1, \quad (3)$$

corresponding to the perfectly no-slip and no-stress boundaries, respectively.

In general, the function $\lambda(\sigma)$ depends on the shape of SHP spots and their geometrical arrangement. To appreciate this dependence one can compare the available analytical solutions for $\lambda(\sigma)$. For instance, for the two-stripe pattern per period (one stripe is no-slip and another is no-stress), one has

$$\frac{\lambda_{\parallel}}{L} = \frac{1}{2\pi} \ln \left[\frac{1}{\sin(\pi(1-\sigma)/2)} \right], \quad (4)$$

where L is the period of the two-stripe pattern, and σ is the SHP surface fraction. The authors of Ref. [12] argue that the relation $\lambda_{\perp} = \frac{1}{2}\lambda_{\parallel}$

* Corresponding author.

E-mail address: alex.skvortsov@defence.gov.au (A.T. Skvortsov).

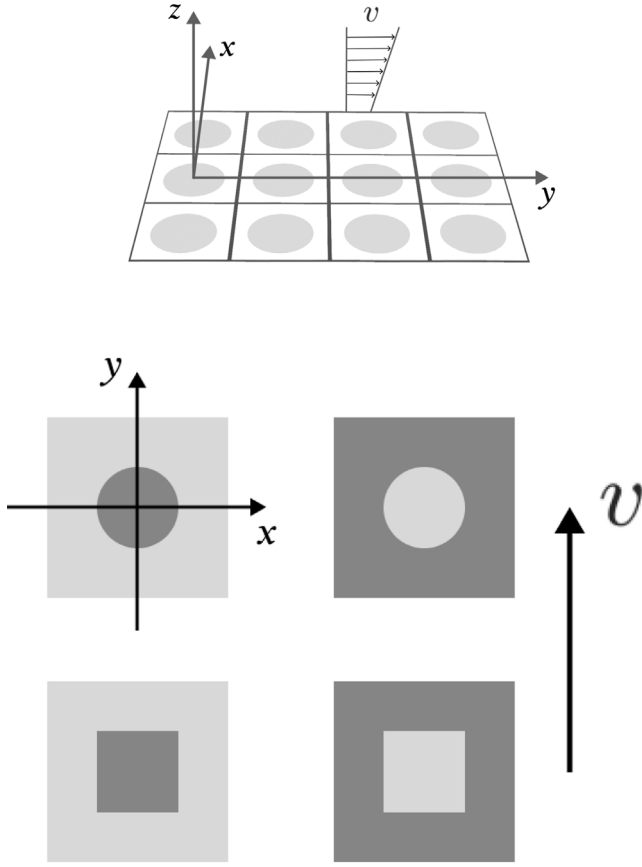


Fig. 1. Sketch of the considered problem, Top: Stokes flow in the y direction over the xy plane coated by periodically repeated disk-shaped spots. Bottom: Examples of periodic cells of two complementary structures of SHP spots (dark) on the no-slip plane (light).

should be approximately valid for any lattice of elongated SHP spots (i.e., a lattice of ellipses with appreciably unequal axes) with respect to their orientation towards the flow.

We note that formula (4) is valid for the entire range $0 < \sigma < 1$ and has the correct limits for $\sigma = 0$ and $\sigma = 1$. This enables an instructive estimation of the effect of SHP texture (in this case its orientation with respect to the flow velocity) for the same surface fraction. Carrying out the similar analysis for a lattice arrangement to predict the effect of the shape and surface fraction of SPH spots is more challenging. The main difficulty is due to the lack of a general formula for $\lambda(\sigma)$ that is valid for the entire range of the SHP surface fraction. Many accurate analytical approximations have been deduced for the sparse limit ($\sigma \ll 1$) [6–8,12–17,19,22,26] but they offer no clear pathways for the extension to the entire range of σ . Derivation and numerical validation of such a formula was the main motivation for the present study. More specifically, we derive an approximate formula for the slip length for two complementary patterns of the SHP texture that is valid for the entire range of σ . We show that, similar to Eq. (4), this formula can provide some upper and lower bounds for the effect of geometrical arrangement of the SHP spots inside the lattice cell on the overall coating performance and thus enables the insightful comparison of various design textures.

It is worth noting that a similar approach capturing the effect of heterogeneity of a surface via a phenomenological parameter introduced in a Robin-type boundary condition (1) is also well-known in electrostatics [27], chemical physics [26,28–32], acoustics, and water wave dynamics [6,33,34] where this parameter is referred to as grid parameter, trapping rate, and blockage coefficient. The similarity in

this approach is due to the overarching analytical framework of the Laplace equation that describes these phenomena.

2. Theory

We deduce the functional form of $\lambda(\sigma)$ for two complementary (or ‘inverse’) configurations of the SHP texture, see Fig. 1. The first configuration is the square lattice of the SHP spots (with boundary condition $dv/dz = 0$) on the no-slip base (with boundary condition $v = 0$). The second configuration is an ‘inverse’ of the first one: it consists of the same lattice but of the no-slip spots ($v = 0$) employed on the SHP base ($dv/dz = 0$).

Similar to Eq. (4) the dimensional arguments imply

$$\frac{\lambda}{L} = F_1(\sigma), \quad (5)$$

$$\frac{\lambda}{L} = F_2(\sigma), \quad (6)$$

for the first and the second case, respectively. Here L is the side length (period) of the lattice, $F_1(\sigma)$ and $F_2(\sigma)$ are dimensionless functions that obey the limits given by Eqs. (2) and (3).

The asymptotic behavior of the functions $F_1(\sigma)$ and $F_2(\sigma)$ as $\sigma \rightarrow 0$ and $\sigma \rightarrow 1$ has been established analytically and numerically [7,8,12–14,17]. In particular,

$$F_1(\sigma) \approx \frac{A}{\sqrt{1-\sigma}} - B, \quad \sigma \rightarrow 1, \quad (7)$$

$$F_1(\sigma) \approx C\sigma^2, \quad \sigma \rightarrow 0, \quad (8)$$

$$F_2(\sigma) \approx H \ln \left[\frac{1}{1-\sigma} \right], \quad \sigma \rightarrow 1, \quad (9)$$

$$F_2(\sigma) \approx P\sigma^{3/2}, \quad \sigma \rightarrow 0, \quad (10)$$

where $A = 3\sqrt{\pi}/16$, $B = 3/(2\pi) \ln(1 + \sqrt{2})$, $C = 3\pi/64$, $H = 1/(3\pi)$, $P = 8/(9\pi^{3/2})$.

The values of A and B are given in Ref. [13] as a part of the solution for the Stokes flow over a square lattice of small no-slip disks lying on the no-stress base. The value of C can be easily derived from Eq. (2.7) of Ref. [7] for the solution for a square lattice of large no-slip square plates with small no-stress gaps between them.

The value of P is given in Refs. [7,8] for the inverse configuration. The value of H is established in Refs. [12,19] for the so-called narrow stripe limit, which corresponds to a lattice of the narrow no-stress flat rings on the no-stress plane as $\sigma \rightarrow 1$, see Fig. 1. The logarithmic singularity in Eq. (9) agrees with the same singularity in Eq. (4).

Our aim is to provide interpolation formulas for $F_1(\sigma)$ and $F_2(\sigma)$ that smoothly match these asymptotics and are valid over the entire range of the surface fraction of SHP spots, $0 \leq \sigma \leq 1$. Motivated by the similar studies for the Laplace equation reported in Refs. [28–30] we propose the following expressions

$$F_1(\sigma) = \frac{\gamma\sigma^2}{\sqrt{1-\sigma}[1 + \alpha\sqrt{1-\sigma} + \beta(1-\sigma)^2]}, \quad (11)$$

$$F_2(\sigma) = \zeta\sigma^{3/2} \ln[\delta + 1/(1-\sigma)], \quad (12)$$

where $\gamma, \alpha, \beta, \zeta, \delta$ are constants to be determined. Matching with Eqs. (7)–(10) leads to the explicit formulas

$$\gamma = A, \quad \alpha = B/A, \quad (13)$$

$$\beta = A/C - B/A - 1, \quad (14)$$

for constants in $F_1(\sigma)$, and

$$\zeta = H, \quad (15)$$

$$\delta = \exp(P/H) - 1, \quad (16)$$

for constants in $F_2(\sigma)$.

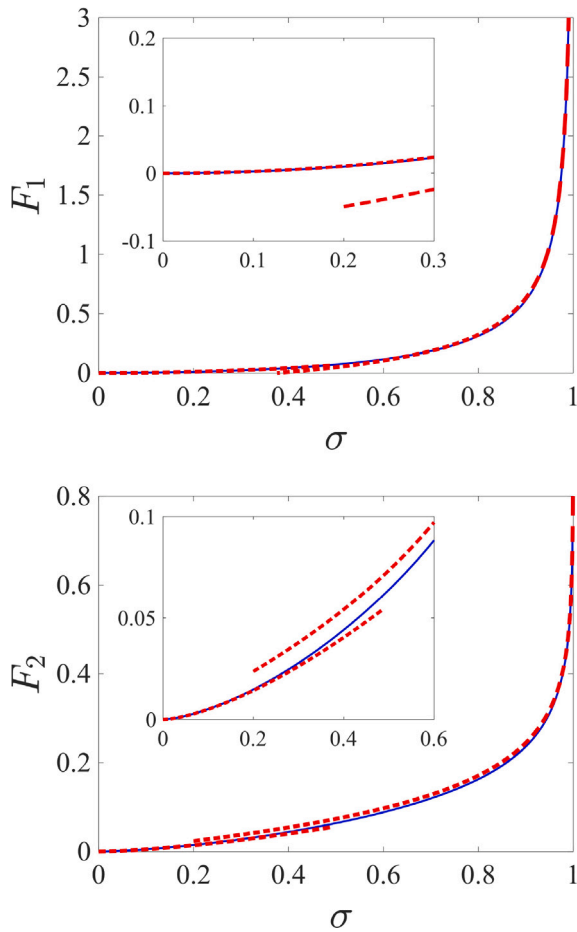


Fig. 2. Top: solid blue line shows Eq. (11), dashed red lines indicate the asymptotes (7), (8). Bottom: solid blue line shows Eq. (12), dashed red lines indicate the asymptotes (9), (10). The inset shows a zoom of the region of small σ . (For interpretation of the references to color in this figure legend, the reader is referred to the web version of this article.)

Formulas (13)–(16) determine explicitly all the coefficients in Eqs. (11), (12) for $F_1(\sigma)$ and $F_2(\sigma)$. Indeed, they eliminate any ‘free’ parameters as all parameters in $F_1(\sigma)$ and $F_2(\sigma)$ are expressed in terms of the values of the constants that were previously derived analytically. These formulas and their excellent agreement with numerical simulations present the main result of the paper. The plots of $F_1(\sigma)$ and $F_2(\sigma)$ are shown in Fig. 2 where the asymptotes of Eqs. (7)–(10) are also presented.

3. Numerical simulations

To validate the proposed expressions for $F_1(\sigma)$ and $F_2(\sigma)$ we performed the numerical simulations of the Couette flow (the flow of a viscous fluid in the space between two planes, one of which is moving parallel to the other with a constant velocity v_0). An open-source, high-order spectral element solver, NEK5000 [35] was used. The Stokes equation with the mixed boundary conditions (no-slip and no-stress) imposed at the $z = 0$ plane was solved to simulate the viscous flow over the SHP surface. The Reynolds number of the flow at $z = h$ is $Re_h = v_0 h / \nu$, where $\nu = \mu / \rho$ is the kinematic viscosity of the fluid and ρ is the fluid density. Parameters v_0 and h were used as the natural scales of velocity and length, respectively, so the Reynolds number $Re_h < 1$ was the only parameter defining the dimensionless numerical model. The convergence tolerance for velocity was set to 10^{-8} .

The total number of hexahedral spectral elements in the range $185 < \mathcal{N} < 305$ was used to resolve the flow above the SHP surface. The

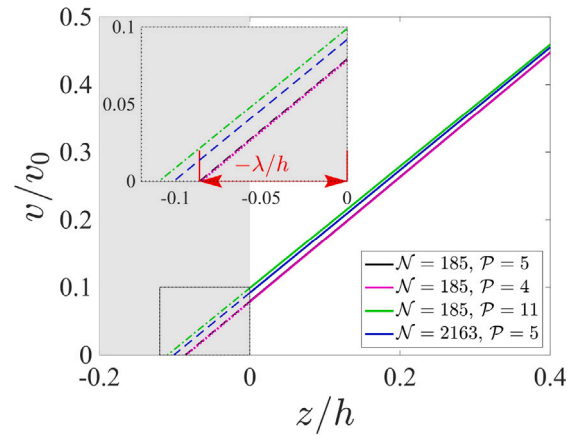


Fig. 3. Plot of the spatially averaged velocity profile for different numbers of spectral elements \mathcal{N} and polynomial orders \mathcal{P} . An inaccuracy of slope estimation leads to an error in estimating λ . The SHP surface is at $z/h = 0$. The gray area corresponds to $z < 0$ or area below the stationary plane.

Lagrange polynomials of order $\mathcal{P} = 5$ were applied as interpolating functions within a spectral element [35]. The slip length λ was estimated by extrapolating the linear velocity profile from far above the SHP surface ($z > 0.4h$) to its intercept on axis $v = 0$ (see Fig. 3). For the lattice of SHP disks in the square cells the maximum of the SHP surface fraction is $\pi/4 \approx 0.785$, so in order to reach the range of higher SHP surface fraction (or no-slip spots for the SHP base) we also ran several configurations with square central spots as shown in Fig. 1. This also allowed us to estimate the effect of the shape of the central spot on the performance of the SHP lattice texture.

To estimate the error of the numerical results we conducted a number of sensitivity studies. These included a grid independence study and a sensitivity study with respect to the Reynolds number value. In particular, we ran the simulations for $Re_h = 1$ and $Re_h = 0.001$ and found that for these Reynolds numbers the slip length is independent of Re_h (the results are not shown), which is in agreement with the theoretical predictions.

Careful refinement of parameters \mathcal{N} and \mathcal{P} was conducted to check the potential issues that might arise from the stress singularities at the edges of the SHP domains. Our study revealed that the profile of the spatially averaged velocity remained the same when the lower-order polynomials $\mathcal{P} = 3$ and $\mathcal{P} = 4$ were applied for interpolation. In turn, an increase in the order of polynomials ($\mathcal{P} > 11$) deteriorated the iterative convergence of the simulations. When more spectral elements \mathcal{N} were used, the required convergence was also more challenging, giving raise to a significantly increased number of iterations. This led to an overestimation of the slip velocity, as shown in Fig. 3. We emphasize that the results presented in this paper correspond to the fully converged simulations.

It is worth noting that the slower convergence of our simulations was not revealed for the conventional no-slip boundary condition on the planes. This is another indication that the slower convergence, and associated numerical errors, seem to be related to the stress singularities at the edges of the SHP domains, as was suggested by one of the reviewers.

4. Results and discussion

Overall, we observed excellent agreement between analytical predictions and the results of numerical simulations (the absolute error of the proposed interpolation was less than 1.5% for F_1 and less than 1.2% for F_2 , see Fig. 4). For different configurations the quality of the interpolation formulas is given in Table 1.

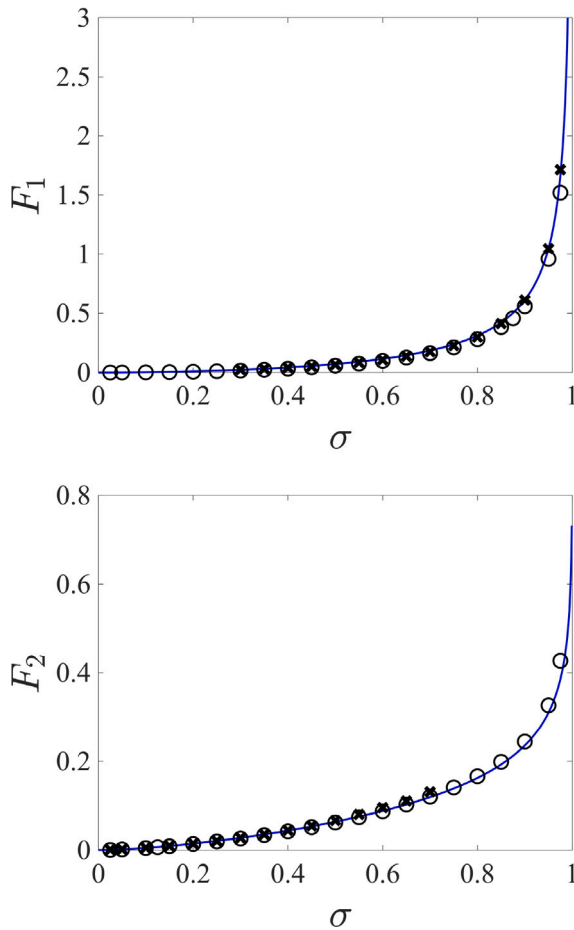


Fig. 4. Plots of $F_1(\sigma)$ and $F_2(\sigma)$ (solid blue lines) validated with numerical simulations (markers). Different markers are used for different shapes of the central spot (o - circle, x - square).

Table 1

Quality of interpolation (coefficient of determination) for the different shapes of central spots in the SHP lattice texture (see Fig. 1).

Shape	F_1	F_2
Circle	99.9%	98.8%
Square	98.7%	99.2%

The similarity of the results for the circle and square shapes of the central spot can be explained by the finding reported in Ref. [16], viz., that the drag force acting on a square zero-thickness plate translated longitudinally is close to that of a circular disk of the same surface area, so for the limit of small σ these plots should be almost identical.

Although not shown here, the accuracy of the interpolation could be further improved (up to 0.5% for F_1 and 0.3% for F_2) if one of the constants in Eqs. (11), (12) was deemed as a free parameter, whose value was evaluated from fitting the numerical data. However, we did not pursue this option. First, it is beyond the scope of the present study, which aims at validating formulas for the slip length deduced from asymptotic expressions; in this light, any free fitting parameter would impose a valid question of the universality of its value. Second, the error of less than 1% of our fully explicit approximation without extra fitting is sufficiently high for most applications.

As the deduced formulas for F_1 and F_2 are interpolation, the values of some parameters in these formulas may vary slightly with the shape of the central spot and the lattice topology. In particular, for a central spot that obeys the symmetry of square (i.e., hexagon) these formulas remain unchanged. Moreover, we expect that variations in

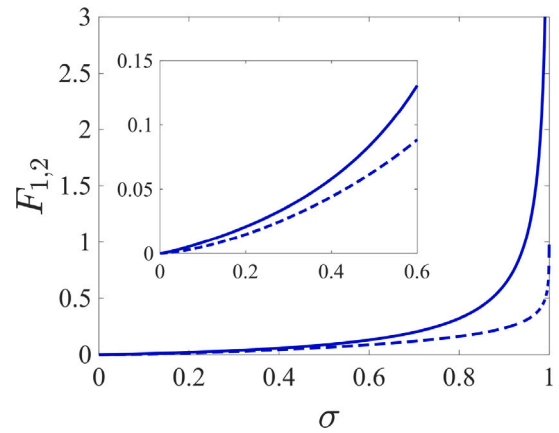


Fig. 5. Comparison of $F_1(\sigma)$ given by Eq. (11) (solid line) and $F_2(\sigma)$ given by Eq. (12) (dashed line). Inset shows a zoom of the region of small σ .

the parameters should be relatively weak since the limiting values of $F_1(\sigma)$ and $F_2(\sigma)$ are primarily determined by the functional form of the universal scaling laws (7)–(10). According to the study of the Laplace equation with mixed boundary conditions in Refs. [28–30], the analysis given here can be extended to include the refined values of parameters in F_1 and F_2 for a different lattice topology and shape of the central spot.

For comparison, the plots of functions F_1 and F_2 are depicted together in Fig. 5. In our view these functions can provide important insights in the optimal design of the SHP coatings which is important for applications. We briefly elaborate on this point.

For our setting of Couette flow the reduction of drag τ can be deduced from a reduction of the effective distance between planes and thus be completely defined in terms of the slip length:

$$\frac{\tau_{coat} - \tau_{flat}}{\tau_{flat}} = \frac{\lambda}{h - \lambda}, \quad (17)$$

so the effect of a SHP texture can be reduced to the analysis of Eqs. (11) and (12). Assume that a SHP coating consists of a lattice of structural elements (e.g., pits or pillars). Within a single lattice cell the structural elements can be distributed with two ‘vastly’ different arrangements: cell-centric (when structural elements are clumped at the center of the cell) and cell-peripheral (when the elements are distributed along the cell perimeter). Then for a given surface fraction σ and all other parameters being fixed the difference in performance between two arrangements reduces to the vertical difference between two lines in Fig. 5 for a given value of σ . Similarly, a horizontal difference between two curves for a prescribed value of λ (i.e., reduction in drag) gives a margin in the required value of σ . If for two similar SHP textures we keep σ the same but change only the period of the lattice L the performance of the new coating is still given by Eqs. (11), (12) but with the different parameter L . Finally, for a given surface fraction σ the parameter λ (i.e. coating performance) is the same provided the products $LF_1(\sigma)$ and $LF_2(\sigma)$ are equal. These arguments enable a simple estimation of the minimum surface fraction of the SHP spots for a given coating performance.

5. Conclusions

In summary, we proposed and validated an interpolation formula for the effective boundary condition (1) with the lumped parameter $\lambda(\sigma)$ given by Eqs. (5) and (6). This formula is valid for the entire range of the SHP surface fraction and allows us to estimate the effect of morphology of the SHP spots on coating performance. We believe that the presented approach can be useful for the rapid ‘what-if’ estimations before proceeding with more comprehensive numerical simulations and prototyping.

CRedit authorship contribution statement

Alexei T. Skvortsov: Writing – original draft, Resources, Methodology, Investigation, Conceptualization. **Denis S. Grebenkov:** Writing – review & editing, Methodology, Investigation, Conceptualization. **Leon Chan:** Validation, Software, Investigation. **Andrew Ooi:** Methodology, Investigation, Conceptualization.

Declaration of competing interest

The authors declare that they have no known competing financial interests or personal relationships that could have appeared to influence the work reported in this paper.

Data availability

Data will be made available on request.

Acknowledgments

The authors thank Ian MacGillivray for useful discussions. This work was partially supported by the DARPA, United States grant PA-23-03-04-DRAG-FP-012, ‘Microstructure riblets with novel coatings for drag reduction applications’.

References

- [1] E. Lauga, M.P. Brenner, H.A. Stone, *Microfluidics: the no-slip boundary condition*, in: *Handbook of Experimental Fluid Dynamics*, Springer, New York, 2007, pp. 1219–1240, Chap. 19.
- [2] J.P. Rothstein, Slip on superhydrophobic surfaces, *Annu. Rev. Fluid Mech.* 42 (2010) 89–109.
- [3] S. Parvate, P. Dixit, S. Chattopadhyay, Superhydrophobic surfaces: insights from theory and experiment, *J. Phys. Chem. B* 124 (2020) 1323–1360.
- [4] E.J. Falde, S.T. Yohe, Y.L. Colson, M.W. Grinstaff, Superhydrophobic materials for biomedical applications, *Biomaterials* 104 (2016) 87–103.
- [5] L. Chen, S. Wang, J. Ding, Y. Wang, P. Bennett, J. Cheng, Q. Yang, D. Liu, Open water characteristics of marine propeller with superhydrophobic surfaces, *Ocean Eng.* 269 (2023) 113440.
- [6] D. Crowdy, Frictional slip lengths and blockage coefficients, *Phys. Fluids* 23 (2011) 091703.
- [7] C. Pozrikidis, Slip velocity over a perforated or patchy surface, *J. Fluid Mech.* 643 (2010) 471–477.
- [8] M. Sbragaglia, A. Prosperetti, Effective velocity boundary condition at a mixed slip surface, *J. Fluid Mech.* 578 (2007) 435–451.
- [9] M.Z. Bazant, Exact solutions and physical analogies for unidirectional flows, *Phys. Rev. Fluids* 1 (2016) 024001.
- [10] D.S. Grebenkov, Diffusion-controlled reactions: An overview, *Molecules* 28 (2023) 7570.
- [11] D.G. Crowdy, Slip length for longitudinal shear flow over a dilute periodic mattress of protruding bubbles, *Phys. Fluids* 22 (2010) 121703.
- [12] A.M.J. Davis, E. Lauga, The friction of a mesh-like super-hydrophobic surface, *Phys. Fluids* 21 (2009) 113101.
- [13] A.M.J. Davis, E. Lauga, Hydrodynamic friction of fakir-like superhydrophobic surfaces, *J. Fluid Mech.* 661 (2010) 402–411.
- [14] C.O. Ng, C.Y. Wang, Stokes shear flow over a grating: Implications for superhydrophobic slip, *Phys. Fluids* 21 (2009) 013602.
- [15] O. Schnitzer, E. Yariv, Resistive-force theory for mesh-like superhydrophobic surfaces, *Phys. Rev. Fluids* 3 (2018) 032201(R).
- [16] O. Schnitzer, E. Yariv, Small-solid-fraction approximations for the slip-length tensor of micropillared superhydrophobic surfaces, *J. Fluid Mech.* 843 (2018) 637–652.
- [17] E. Yariv, Effective slip length for longitudinal shear flow over partially invaded grooves: Small solid-fraction approximations, *Phys. Rev. Fluids* 8 (2023) L012101.
- [18] J.R. Philip, Flows satisfying mixed no-slip and no-shear conditions, *Z. Angew. Math. Phys.* 23 (1972) 353–372.
- [19] C. Ybert, C. Barentin, C. Cottin-Bizonne, P. Joseph, L. Bocquet, Achieving large slip with superhydrophobic surfaces: Scaling laws for generic geometries, *Phys. Fluids* 19 (2007) 123601.
- [20] M.Z. Bazant, O. Vinogradova, Tensorial hydrodynamic slip, *J. Fluid Mech.* 613 (2008) 125–134.
- [21] F. Feuillebois, M.Z. Bazant, O.I. Vinogradova, Effective slip over superhydrophobic surfaces in thin channels, *Phys. Rev. Lett.* 102 (2009) 026001.
- [22] A.V. Belyaev, O.I. Vinogradova, Effective slip in pressure-driven flow past super-hydrophobic stripes, *J. Fluid Mech.* 652 (2010) 489–499.
- [23] A.T. Skvortsov, D.S. Grebenkov, L. Chan, A. Ooi, Slip length for a viscous flow over spiky surfaces, *Europhys. Lett.* 143 (2023) 63001.
- [24] C. Lee, Chang-Hwan Choic, Chang-Jin Kim, Superhydrophobic drag reduction in laminar flows: a critical review, *Exp. Fluids* 57 (2016) 176.
- [25] Z.Q. Tang, T. Tian, P.J. Molino, A. Skvortsov, D. Ruan, J. Ding, Y. Li, Recent advances in underwater superhydrophobic materials development for maritime applications, *Adv. Sci.* (2024) e2308152.
- [26] A. Skvortsov, Mean first passage time for a particle diffusing on a disk with two absorbing traps at the boundary, *Phys. Rev. E* 102 (2020) 012123.
- [27] D.P. Hewitt, L.J. Hewitt, Homogenized boundary conditions and resonance effects in Faraday cages, *Proc. R. Soc. Lond. Ser. A Math. Phys. Eng. Sci.* 472 (2016) 20160062.
- [28] Y.A. Makhnovskii, A.M. Berezhkovskii, V.Y. Zitserman, Homogenization of boundary conditions on surfaces randomly covered by patches of different sizes and shapes, *J. Chem. Phys.* 122 (2005) 236102.
- [29] A.M. Berezhkovskii, M.I. Monine, C.B. Muratov, S.Y. Shvartsman, Homogenization of boundary conditions for surfaces with regular arrays of traps, *J. Chem. Phys.* 124 (2006) 036103.
- [30] C.B. Muratov, S.Y. Shvartsman, Boundary homogenization for periodic arrays of absorbers, *Multiscale Model. Simul.* 7 (1) (2008) 44–61.
- [31] L. Dagdug, A.T. Skvortsov, A.M. Berezhkovskii, S.M. Bezrukov, Blocker effect on diffusion resistance of a membrane channel. Dependence on the blocker geometry, *J. Phys. Chem. B* 126 (32) (2022) 6016–6025.
- [32] D.S. Grebenkov, A.T. Skvortsov, Boundary homogenization for target search problems, 2023, arXiv:2310.14322.
- [33] P.A. Martin, A.T. Skvortsov, Scattering by a sphere in a tube, and related problems, *J. Acoust. Soc. Am.* 148 (2020) 191.
- [34] P.A. Martin, A.T. Skvortsov, On blockage coefficients: flow past a body in a pipe, *Proc. R. Soc. Lond. Ser. A Math. Phys. Eng. Sci.* 478 (2022) 20210677.
- [35] P. Fischer, J. Kruse, J. Mullen, H. Tufo, J. Lottes, S. Kerkemeier, Nek5000: Open Source Spectral Element CFD Solver, Argonne National Lab., Argonne, USA, 2008.